THE SOLAR ATMOSPHERE AND THE STRUCTURE OF ACTIVE REGIONS

under the direction of

P.A. Sturrock

Semiannual Report No. 7

January 1, 1975 - June 30, 1975

for NASA Grant NGL 05-020-272

National Aeronautics and Space Administration

Washington, D.C. 20546

August 1975

Institute for Plasma Research
Stanford University
Stanford, California

STAFF

NASA Research Grant NGL 05-020-272

for the period

January 1, 1975 - June 30, 1975

PRINCIPAL INVESTIGATOR

P.A. Sturrock, Professor

FACULTY

V. Petrosian

RESEARCH ASSOCIATES

C.W. Barnes

B.J. Lipa

C.E. Newman

RESEARCH ASSISTANTS

S.K. Antiochos

J.W. Knight

1. Thermal Instability in Loop Prominences

(S.K. Antiochos and P.A. Sturrock)

In our previous report we commented that in order for thermal instability to be important in loop prominences, it is necessary that radiation be the dominant cooling mechanism. In our model this is true because the magnetic field acts to decrease the conductive losses to the chromosphere. The reduction of conduction cooling is due to two effects: the curvature of the field increases the effective distance between the hot plasma and the chromosphere so that the heat flux is reduced; and the area of a loop increases reapidly with height so that for a large ratio of top area to base area, the flow of heat out of the ends of the loop is constricted.

In order to investigate this effect quantitatively, we have considered a simple model in which the plasma remains stationary while cooling. Assuming that the temperature is high ($\sim 10^7$ K), gravity and radiation losses can be neglected. If s measures the distance along the loop measured from the top (Figure 1), the fluid equations reduce to

$$n = n(s) \tag{1}$$

$$p = p(t) \tag{2}$$

and the heat equation

$$\frac{3}{2} p^{-1/2} \frac{d}{dt} p(t) = \frac{10^{-6}}{A(s)} \frac{d}{ds} \left(A \frac{d}{ds} \beta(s) \right) ; \tag{3}$$

where

$$\beta(s) = \frac{2}{7} \left[\frac{T(t,s)}{p(t)} \right]^{7/2} . \tag{4}$$

For boundary conditions, we assume that

$$p(o) = p_o \tag{5}$$

$$T(s_b,t) = T_b \approx 0 \tag{6}$$

and

$$\frac{d\,T}{ds}\,(0,t) = 0 \quad . \tag{7}$$

The latter condition follows from the symmetry of the loop, since we expect the heat flux to vanish at the top. The variables s and t are separated in equation (3), which can therefore be integrated directly to obtain

$$p(t) = p_o\,(1 + t/\tau)^{-2/5} \tag{8}$$

and

$$T(\chi,t) = T(o,o)(1 + t/\tau)^{-2/5}\left[1 - \frac{\sin^2\chi}{\cos^4\chi}\,\frac{\cos^4\chi_b}{\cos^2\chi_b}\,\gamma_1(x)\right] \tag{9}$$

where the spatial variable has been changed from the distance s to the angle χ shown in Figure 1. The function $\gamma_1 \approx 1$ for $0 \leq \chi \leq \pi/2$, so that it can be neglected. The cooling time scale τ can be calculated using the boundary conditions,

$$\tau = \frac{21}{10}\,\frac{p_o\,H_o^2}{10^{-6}\{T(o,o)\}^{7/2}}\,\frac{\sin^2\chi_b}{\cos^4\chi_b} \quad . \tag{10}$$

To determine the effect of the area factor on the cooling, we have used the results above to compare the cooling time scale and outward heat flux of a loop of base area A_b to those of a loop of constant area but of exactly the same length. From equation (10) we obtain

$$\frac{\tau}{\tau_c} = \left(\frac{H_o}{s_b}\right)^2 \frac{\sin^2 \chi_b}{\cos^4 \chi_b} \tag{11}$$

where τ_c is the cooling time of a constant-area loop, and

$$\frac{F}{F_c} = \left(\frac{s_b}{H_o}\right) \frac{\cos \chi_b}{\sin \chi_b} \tag{12}$$

for the ratio of the outward heat fluxes. The right hand sides of equations (11) and (12) can be expressed as functions of the base area only by using

$$\frac{s_b}{H_o} = \frac{\nu}{2}\sqrt{3\nu^2 + 1} + \frac{\ell n(\sqrt{3}\ \nu + \sqrt{3\nu^2 + 1})}{2\sqrt{3}} \tag{13}$$

and

$$A_b = \frac{(1 - \nu^2)^3}{\sqrt{3\nu^2 + 1}} \tag{14}$$

where

$$\nu = \sin \chi_b \quad . \tag{15}$$

Figures 2 and 3 show the dependence of τ/τ_c and F/F_c on A_b. We note that for small base areas the cooling time is greatly increased.

Of course these results are not valid for very small areas since radiative cooling will begin to dominate conductive cooling. In order to accurately determine the heat losses, we ran several cases through our computer code (Antiochos and Sturrock, 1974). The results are shown in Figure 6. In each case the loop plasma was assumed to be initially at rest with a uniform temperature and density profile of 10^7 K and 10^{11} cm^{-3} respectively. The length of the loop from the top to the chromosphere was adjusted to be 5×10^9 cm., while the values of A_b

that were used varied from 1/50 to 1 (corresponding to a loop of constant area).

From Figure 4 we notice that, as expected, loops of small base area have initially a lower cooling rate. However, after a large fraction of the loop energy has been lost the situation is reversed and loops of large base area cool more slowly. This is due to the following effect. At the later stages of cooling, the heat losses are essentially all radiative since conduction is negligible for low temperatures. Loops with small base area cool mainly by radiation and they tend to retain a uniform temperature and density profile as they cool. However, loops of large base area have significant conductive losses out of the base, and they tend to form large temperature differences between the feet and the top of the loop. Therefore, in order to maintain pressure balance the density of the hot plasma decreases, thereby lowering the cooling rate.

This effect also occurs in thermal instability. The appearance of condensations does not necessarily mean that the loop cools faster. The cooling rate does increase at the onset of instability, but after a condensation has formed and absorbed a significant fraction of the plasma, the hot gas remaining has a lower density and cooling rate.

By incorporating this work with our previous results (Antiochos and Sturrock, 1975) on the thermal instability of loop plasma, we hope to explain the observed longevity of condensations in active prominences.

References

Antiochos, S.K. and Sturrock, P.A. 1974, NASA Semiannual Report No. 5.

Antiochos, S.K. and Sturrock, P.A. 1975, NASA Semiannual Report No. 6.

Figure Captions

1. Geometry of loop prominences
2. Ratio of conductive cooling rates τ/τ_c for a dipole loop to that for a constant area loop of the same length as a function of A_b, the ratio of base area to area at the top of the dipole loop.
3. Ratio of outward heat fluxes F/F_c as a function of A_b.
4. Fraction of energy left as a function of time for several loops with different base areas.

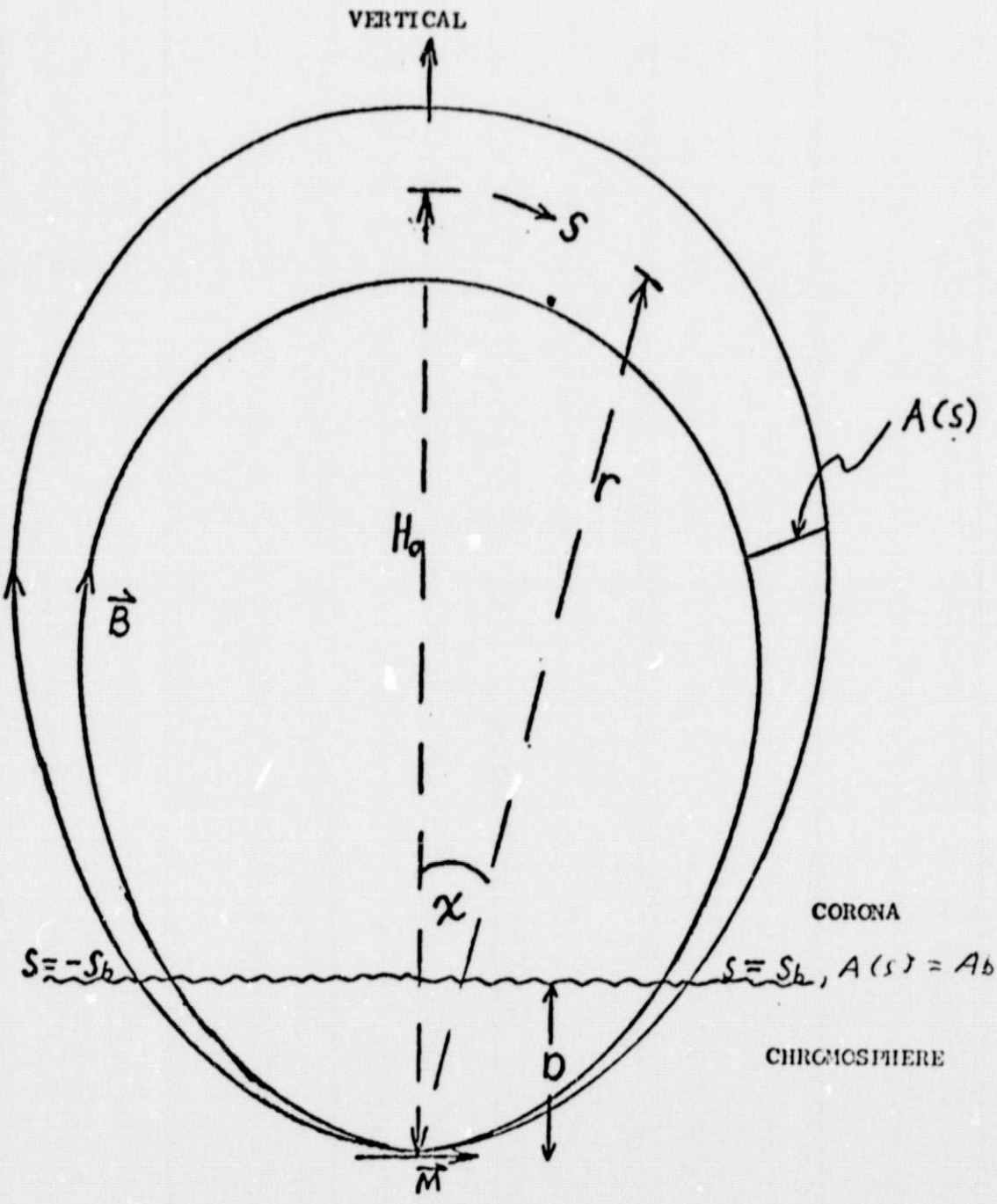

MODEL LOOP

Figure 1

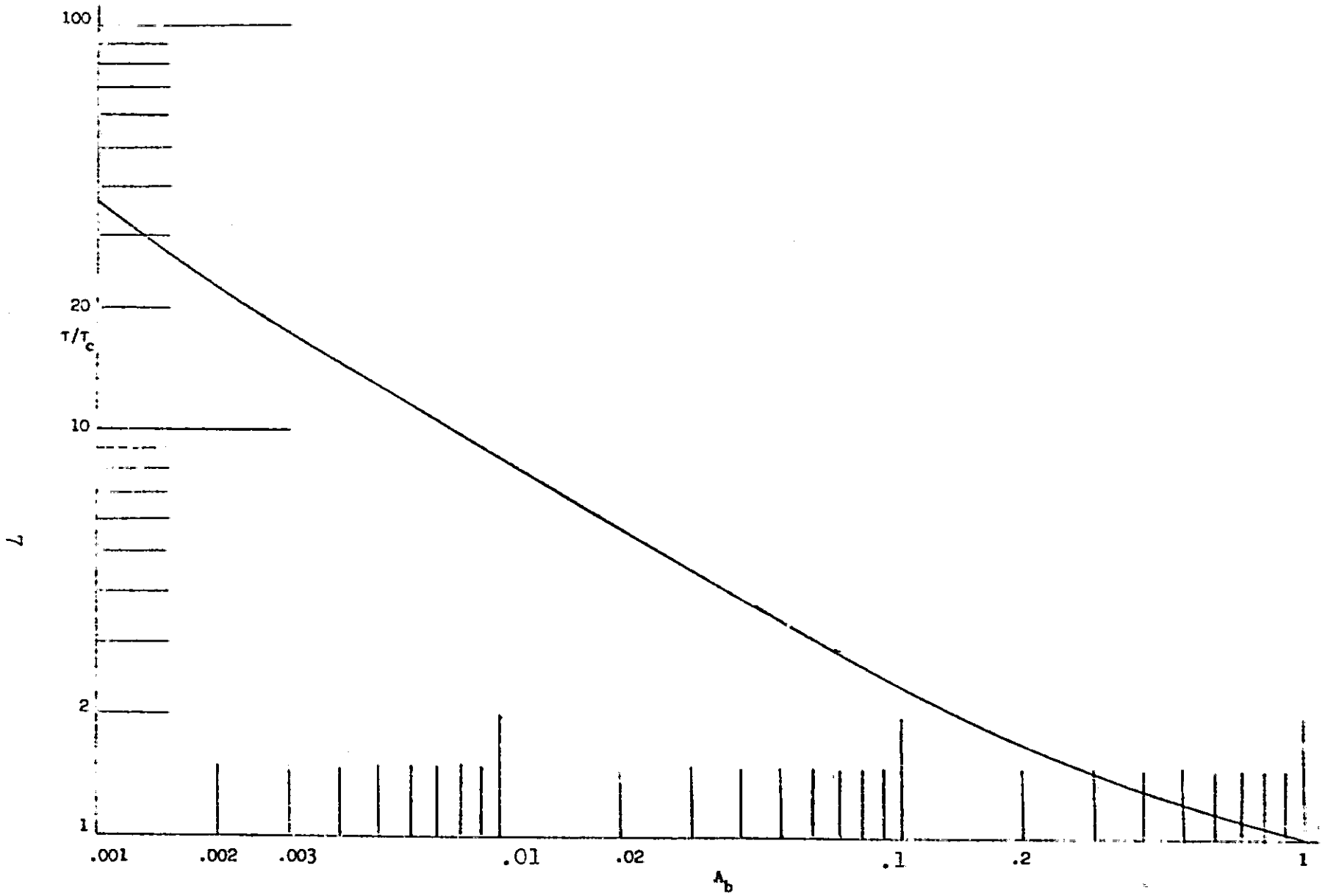

Figure 2

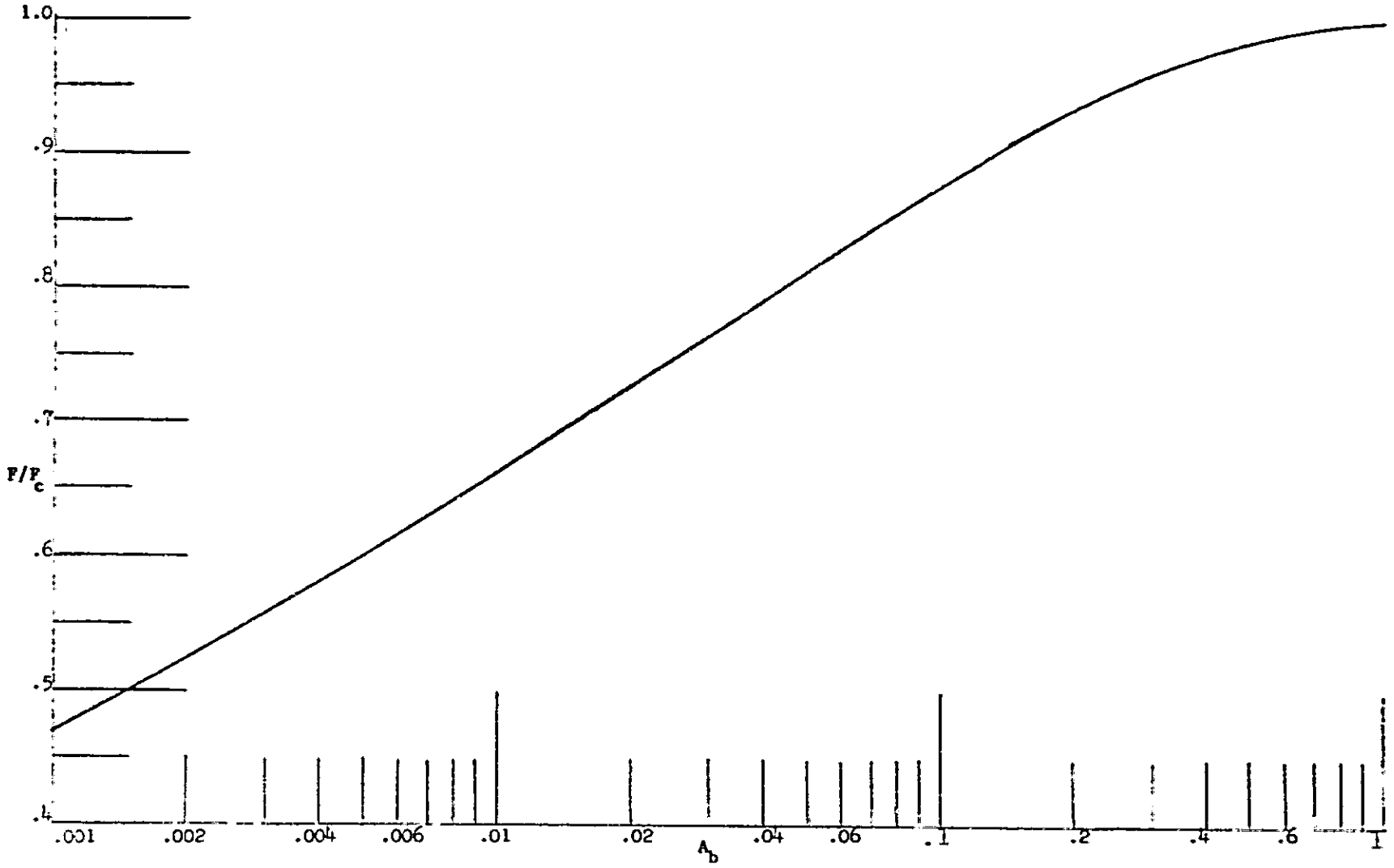

Figure 3

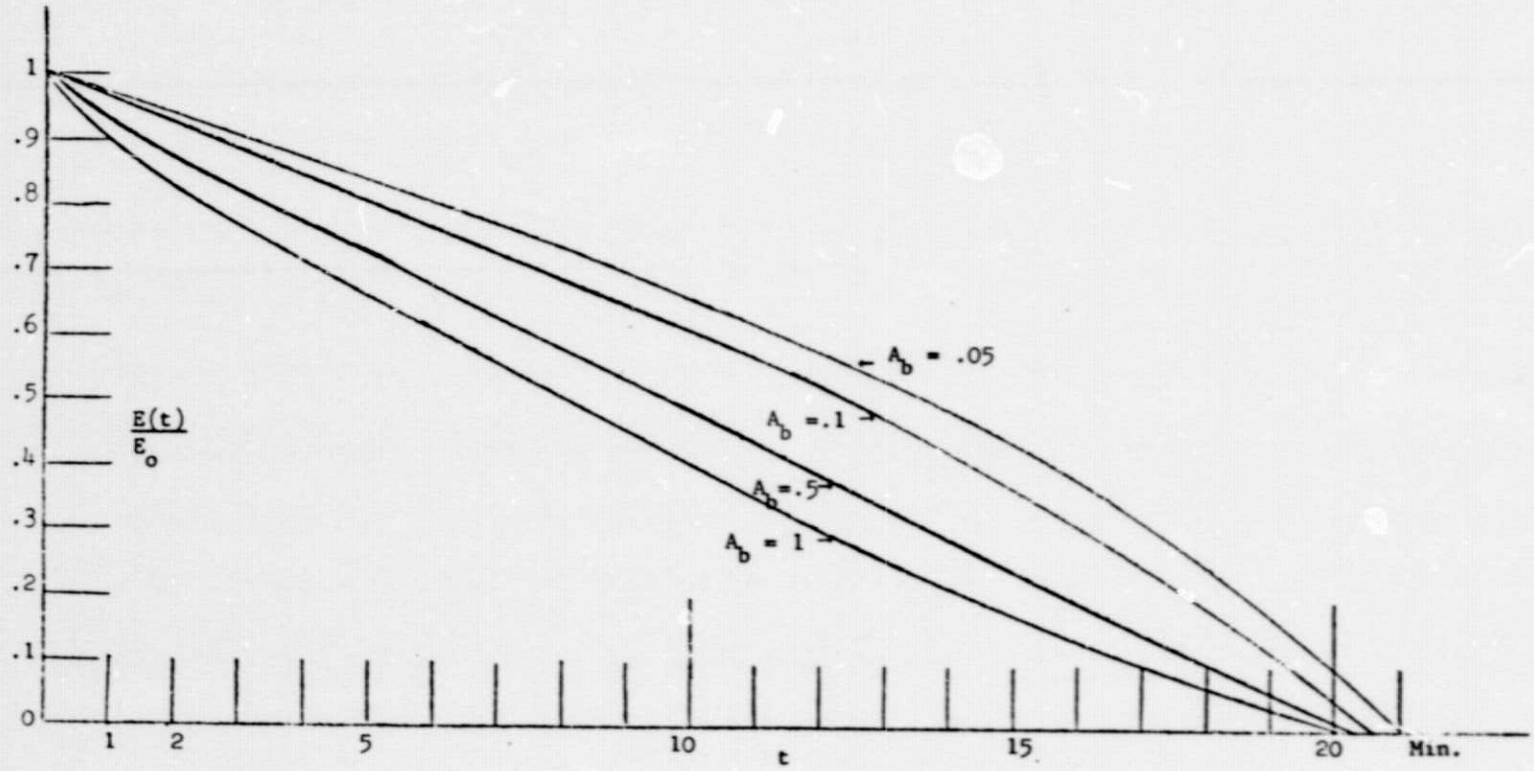

Figure 4

2. Force-Free Magnetic Fields and Their Role in Solar Activity
(C.W. Barnes)

During the present period, further calculations have been made using the spherical version of our force-free-field calculator discussed in the last report. Our model places a perfect conductor at the maximum radius of the mesh which prevents field lines from extending beyond that point. As long as the field strength there is small, this approximation does not introduce significant error. The cases reported last time showed a flattening of the field lines against the boundary for large shear situations. We have increased the number of mesh points treated in the code so as to alleviate this problem. Also the mesh now extends from pole to pole, since it was found that field lines extend well into the southern hemisphere even though created near 45° N latitude. The new mesh is 177 cells in $\ln r$ and 129 cells in θ. With the same length-to-width ratio of cell sides (0.7) as used before, the radius extends now to 20 surface radii instead of 5.2 radii. As before, the relaxation algorithm can be applied to the whole mesh or a coarser subset of it (covering the same physical region). The coarser meshes are used initially, with the finer meshes used for final convergence to the solution.

The results of a run which duplicates the surface conditions treated in the previous report are shown in Figures 1 - 4. The field lines are shown along with lines of constant shear (longitude). Both radius and latitude are plotted on linear scales instead of the radial logarithmic scale on which the calculation is performed. The

four figures show results for shear angles of 0., $\pi/2$, π and 2π radians. The large degree to which the lines billow out with shear can be easily seen. It is also apparent that even with the outer boundary at 20 radii, the field lines for large shear eventually push against it. Figure 5 shows the variation of stored energy with maximum shear angle γ for these cases and compares it with that of the open-field-line case. It can be seen that the mesh fineness causes some variation of stored energy due to inaccurate representation of the α function with coarse meshes. The solutions were all self-consistent however, with calculated fields being very nearly force-free even with the coarsest mesh.

We have also performed some calculations of fields in which a single field line is distorted outward at a single point. Figure 6 shows the field pattern in the case with maximum shear = 2π. The local distortion of the α = 0.65 line can be seen. The result of this calculation unfortunately did not tell us whether the field energy increased or decreased with distortion, only that the change was small indeed (less than 1%). Distorting the same field line in a case of small shear ($\gamma_{max} = \pi/4$), showed the same shallow energy dependence with a small increase in energy. Both of these cases had difficulty converging stably. We therefore feel that this approach will not be as useful as we had hoped.

At present, we are trying a different approach to field line distortion. If the center of shear is placed at the equator and is made a line of symmetry, the equator becomes one of the model boundaries upon which we can arbitrarily set the value of the α-function. We feel that it will be easier to achieve convergence to a solution with

larger distortions of the fields outward. If this is the case, we will be in a position to better understand the stability properties of cases with large shear angle.

Figure Captions

Figure 1: Magnetic field lines (contours of α) for a line dipole at 45° N latitude on a sphere. The pattern is mapped onto a rectangle mesh with latitude plotted horizontally and radius plotted (logarithmically) vertically. The maximum shear in this case is small (0.1 radian).

Figure 2: Magnetic field lines (contours of α) and lines of constant shear (γ) for the case $\gamma_M = \pi/2$.

Figure 3: Magnetic field lines (contours of α) and lines of constant shear (γ) for the case $\gamma_M = \pi$.

Figure 4: Magnetic field lines (contours of α) and lines of constant shear (γ) for the case $\gamma_M = 2\pi$.

Figure 5: Plot of relative stored magnetic energy versus maximum shear angle. Also shown is the energy associated with a dipole with completely open field lines.

Figure 6: Magnetic field lines (α) and lines of constant shear (γ) for the case $\gamma_M = 2\pi$ which has been artificially distorted. The value of α has been adjusted to represent the physical outward movement of a field line (that which shows a cusp).

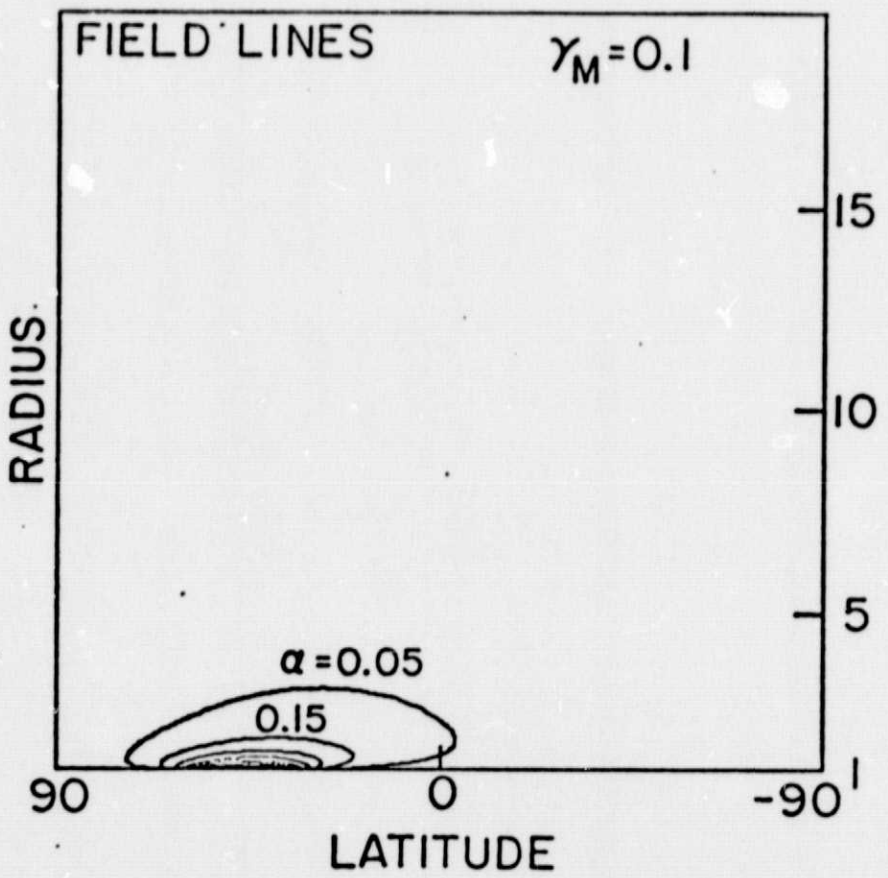
FIELD LINES
γ_M=0.1
RADIUS
15
10
5
1
α=0.05
0.15
90
0
-90
LATITUDE

Figure 1

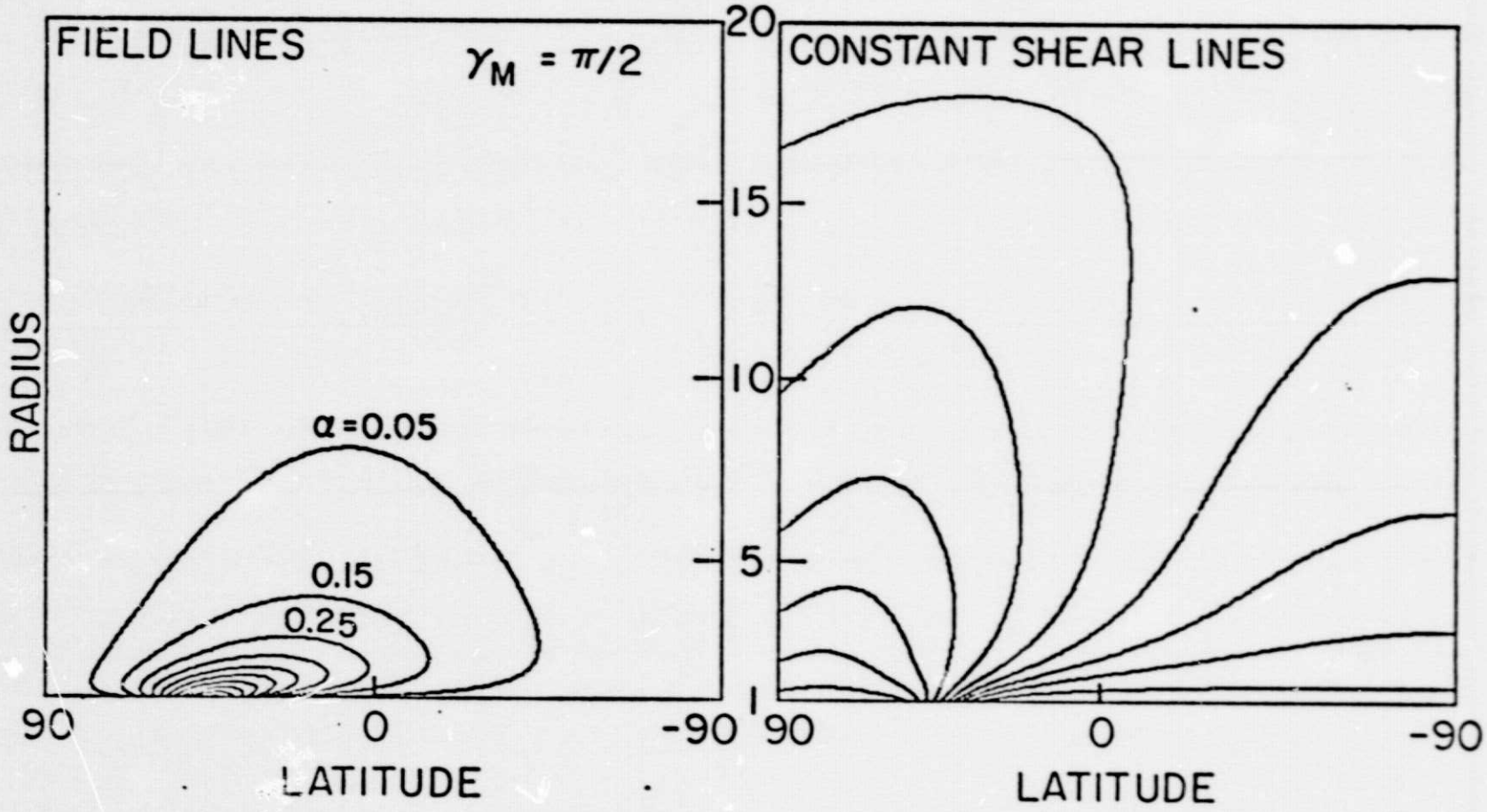
FIELD LINES
$\gamma_M = \pi/2$
CONSTANT SHEAR LINES
RADIUS
20
15
10
5
1
α=0.05
0.15
0.25
90
0
-90
LATITUDE
90
0
-90
LATITUDE

Figure 2

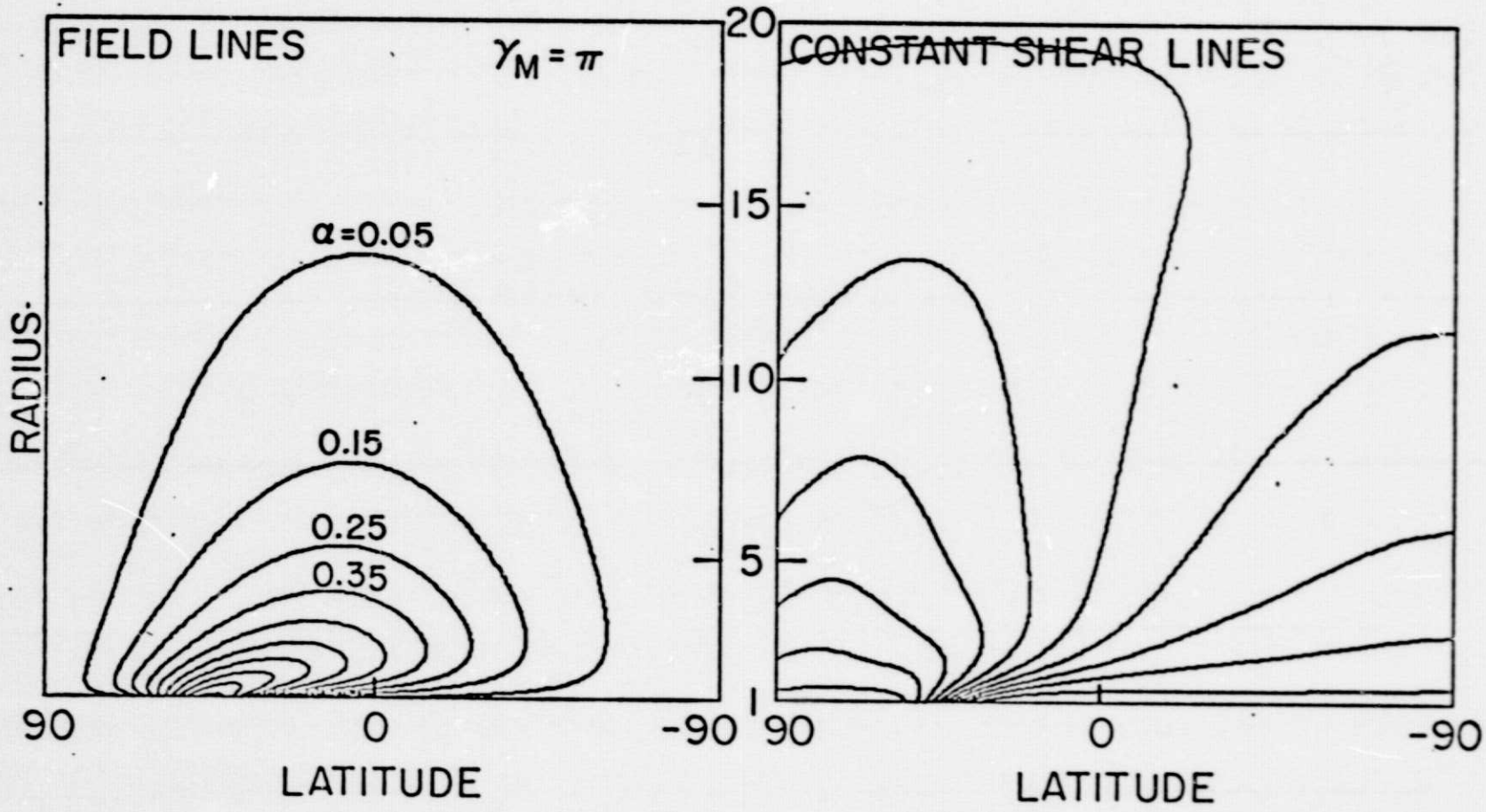
FIELD LINES
$\gamma_M = \pi$
α=0.05
0.15
0.25
0.35
RADIUS
20
15
10
5
1
90
0
-90
LATITUDE
CONSTANT SHEAR LINES
90
0
-90
LATITUDE

Figure 3

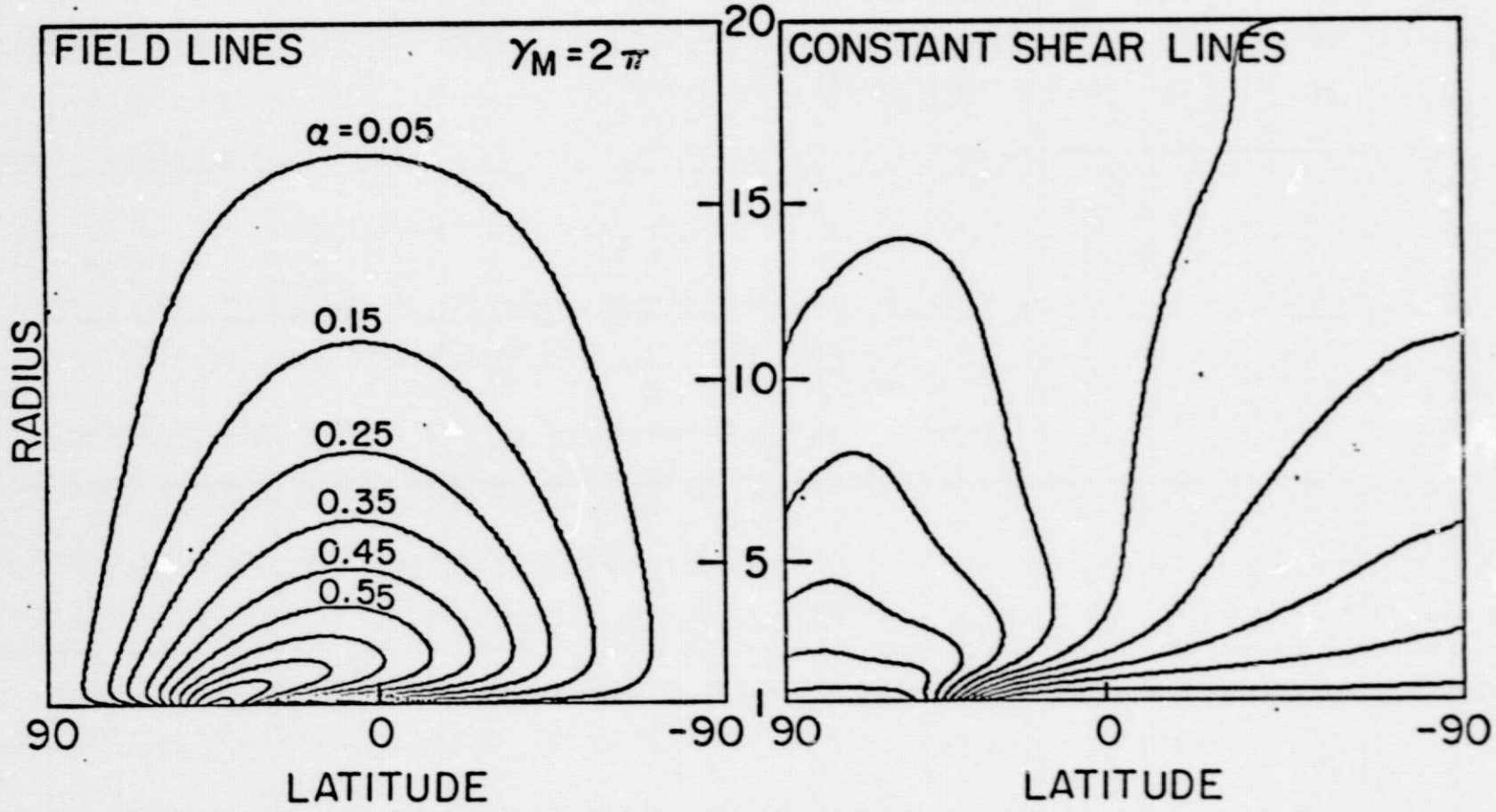
FIELD LINES
$\gamma_M = 2\pi$
$\alpha = 0.05$
0.15
0.25
0.35
0.45
0.55
RADIUS
20
15
10
5
1
90
0
-90
LATITUDE
CONSTANT SHEAR LINES
90
0
-90
LATITUDE

Figure 4

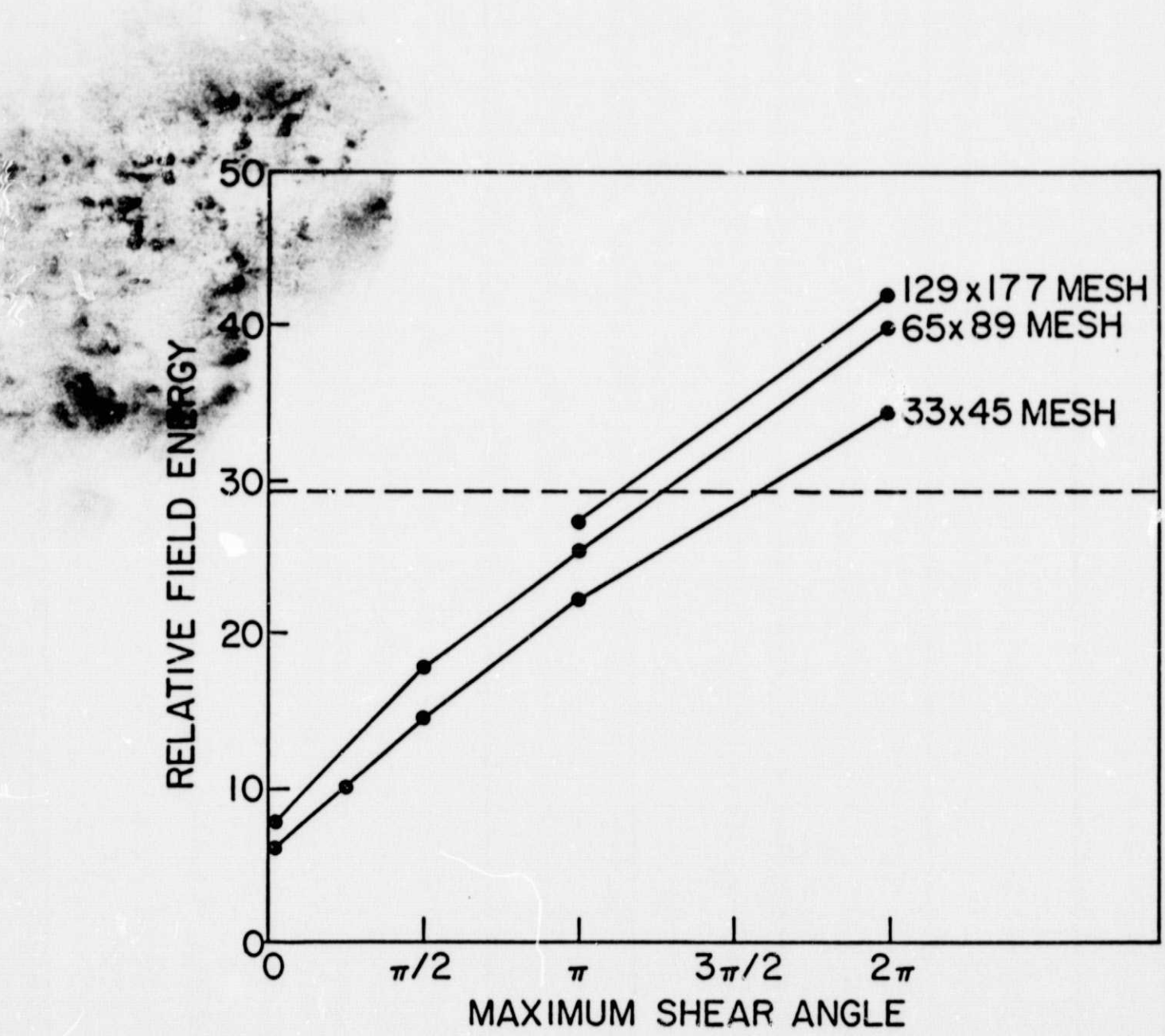
RELATIVE FIELD ENERGY
50
40
30
20
10
0
129 x 177 MESH
65x 89 MESH
33x45 MESH
0
π/2
π
3π/2
2π
MAXIMUM SHEAR ANGLE

Figure 5

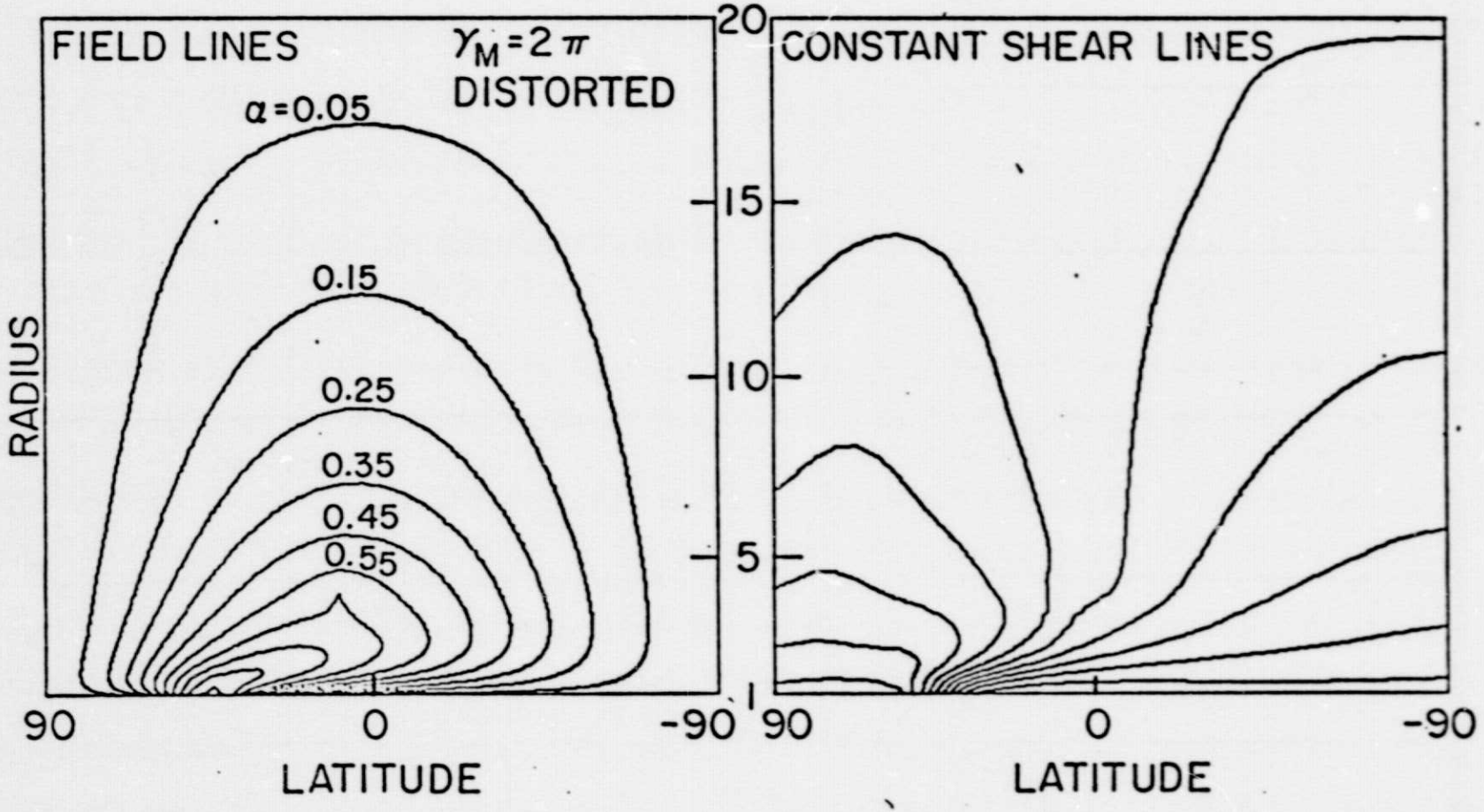
FIELD LINES
$\gamma_M = 2\pi$
DISTORTED
α=0.05
0.15
0.25
0.35
0.45
0.55
RADIUS
20
15
10
5
1
90
0
-90
LATITUDE
CONSTANT SHEAR LINES
90
0
-90
LATITUDE

Figure 6

3. Aircraft Accident Study
(J.W. Knight and P.A. Sturrock)

As we indicated in our previous progress report, we have nearly completed our study of the possibility that the aircraft accident rate may be affected by solar related phenomena. This study has so far produced provocative but not conclusive results. There are two extensions of our previous work which might make the results more clear-cut.

Wilcox et al. (1973) found a dependence of the northern hemispheric vorticity area index on the interplanetary magnetic field structure. This effect was evident only for the winter months. If a connection between the aircraft accident rate and some solar related phenomena existed only for the winter months, our previous methods of analysis might not reveal it. Because the average accident rate is lower in the winter, any effect on the aircraft accident rate present only in the winter could be masked by the larger number of unaffected accidents in the summer months. To compute least-squares spectra for non-continuous data sets, a major modification of our computer code which generates these spectra was necessary. We have recently completed this modification, and we intend to analyze the aircraft accident and a_p data to ascertain if any seasonal effects are present.

The earth's orbit is not circular, but slightly elliptical. This causes the apparent rotation period of the sun to vary through the year (Graf, 1974). The fact that the apparent rotation period of the sun varies through the year could make any solar-related signal present in the aircraft accident data more difficult to detect than a purely periodic signal. It is reasonably easy to derive, to first order in

ϵ the eccentricity of the earth's orbit, a simple formula for the amount φ the sun appears to have rotated as a function of time. If time is measured from perihelion, we find

$$\varphi = \omega_{sid}\, t - \omega_o t - 2\epsilon \sin \omega_o t = \omega_{syn}\, t - 2\epsilon \sin \omega_o t \quad , \qquad (1)$$

where ω_{sid} is the sideral angular velocity of the sun, ω_o is the average angular velocity of the earth in its orbit, and ω_{syn} is the average apparent (synodic) angular velocity of the sun. It is relatively straightforward to modify the formula used to calculate the least squares spectrum to account for the eccentricity of the earth's orbit to first order in ϵ. We simply vary the parameters a, b and ω to minimize

$$V_3 = \sum_{n=1}^{N} [x_n - \langle x \rangle - a \cos (\omega t - 2\epsilon \sin \omega_o t) - b \sin (\omega t - 2\epsilon \sin \omega_o t)]^2 \qquad (2)$$

where x_n are the data, $\langle x \rangle$ is the average of the data, and N is the number of data analyzed. The significance of the least-square fits generated in this manner may be assessed in the same way as we have previously calculated significance estimates for least-squares spectra. We are in the process of modifying the computer code used to calculate least-squares spectra to calculate least-squares "eccentricity corrected" spectra.

We have used the computer codes written for the aircraft accident study to analyze the vorticity area index used by Wilcox et al. (1973) in their study of possible connections between the interplanetary magnetic field structure and terrestrial weather. Preliminary results of this analysis are discussed in Section 4 of this report.

References

Graf, W. 1974, Solar Phys. 37, 257.

Wilcox, J.M., Scherrer, P.H., Svalgaard, L., Roberts, W.O., and Olson, R.H. 1973, Science 180, 185.

4. Solar Effects on Terrestrial Weather
(J.W. Knight and P.A. Sturrock)

It has long been known that geomagnetic disturbances tend to recur after approximately 27 days (Maunder, 1904a, 1904b; Chree and Stagg, 1927; Bartels, 1932). More recently, this effect has been associated with the rotation of the interplanetary magnetic field structure (Ness and Wilcox, 1967; Schatten and Wilcox, 1967; Wilcox, 1968; Wilcox and Coburn, 1972). Evidence for some relation between the interplanetary magnetic field structure and terrestrial weather has also been reported (Wilcox et al., 1973; Wilcox et al., 1975). The interplanetary magnetic field is usually characterized by either two or four sectors, and this pattern rotates with a fairly well defined period of 27.1±.1 days (Wilcox, 1968). The presence of a periodicity leads naturally to the use of spectral analysis as an independent test of the reported association between the interplanetary magnetic field structure and terrestrial weather. We have obtained data for the vorticity area index used by Wilcox and his colleagues (Wilcox et al., 1973) in their analysis.

Both the G_p and vorticity area indices exhibit annual variations and long term trends. Both data sets have been normalized to remove these variations. We have calculated the least-squares spectrum of the vorticity area index and compared it with the least-squares spectrum of the G_p index. The comparison was accomplished by tabulating the lesser of the two F statistics for the two spectra as a function of period, and searching for peaks in this "comparison spectrum". The five largest peaks in the comparison spectrum are displayed in Table 1.

The largest peak occurred at a period of 27.49 days. We may use the F statistic to determine the probabilities that the calculated reductions in variance are due to chance. Following Abramowitz and Stegun (1970), we find the probability that the fit at 27.49 days is due to chance for the G_p spectrum is $\sim 1.2 \times 10^{-4}$ and for the vorticity is $\sim 1.2 \times 10^{-5}$. The F statistic calculated from the data is distributed only approximately as $F_{2,N-3}$, so using such low probability estimates is probably not justified. We therefore arbitrarily use the lowest probability tabulated by Abramowitz and Stegun (1970) for the F distribution which is 10^{-3}. If the G_p and vorticity indices are independent, then the probability that both indices would exhibit fits of this significance at the same period is 10^{-6}. Even if this estimate is valid, it is not correct to use it since the period of 27.49 days was not chosen a priori, but inferred from the data. It is more appropriate to assess the probability of finding one peak close to the "target" period of 27.1 days. Choosing the range in period to be 27.1±.4 days so that the observed peak is just included in the range is also improper. Rather, we choose the range of observed synodic rotation periods of the photosphere of the sun, 26.87 - 28.98 days (Newton and Nunn, 1951). The least-squares fits were calculated for 22 periods in this range. The probability of obtaining at least one of 22 probability estimates as small as 10^{-6} is $\leq 2.2 \times 10^{-5}$ if all of the periods are independent. This is not the case, however, so the validity of the estimate is not clear-cut.

The probability estimates calculated from the F statistic are unrealistically small and setting a lower limit of 10^{-3} is not a very satisfactory procedure. We therefore have also calculated an empirical

probability estimate. The F statistics for all 1971 periods analyzed were ranked, and the probability of each fit estimated to be the rank of the fit divided by the total number of periods for which fits were calculated. To compare the spectra, the larger of these two probability estimates was tabulated as a function of period. The five most significant peaks in this comparison spectrum are displayed in Table 2. There were two periods with probabilities as low as or lower than the probability for the 27.49 day period. However, all three probabilities were close together and the next most significant peak had a probability estimate approximately twice as large. If we combine the two empirical probability estimates in the same manner as the estimates from the F test, we find that the peak at 27.49 days has the smallest probability estimate ($\sim 3 \times 10^{-5}$) of any of the periods analyzed by more than a factor of two. Again we must compensate for the a posteriori choice of the period. The empirical probability estimate that the observed result was produced by chance is $\leq 6.6 \times 10^{-4}$.

The assumption that the G_p and vorticity indices are independent is probably not justified. However, it is difficult to estimate the probability that the calculated fits would appear in both spectra by chance without some similar assumption. An alternate procedure is to assume that the relationship between the G_p index and the interplanetary magnetic field structure is sufficiently well established that we may use the G_p spectrum to establish a rotation period. We may then accept the probability estimates for the 27.49 day period in the vorticity spectrum. These estimates are $< 10^{-3}$ and $\sim 1.4 \times 10^{-2}$ for the F test and empirical probability estimates respectively. It is possible that

using the G_p spectrum to select a rotation period is not appropriate. In this case, we may base our estimates only on the vorticity spectrum, and the probability that the calculated fit would occur in one of 22 periods is quite high (> 25%) for the empirical probability estimates.

We have attempted to assess the significance of the observed peaks under various assumptions. The results vary from greater than 99.9% to less than 75%. We feel the former estimate is unrealistically high and the later unrealistically low. We feel the most reasonable procedure of the methods we have described is to accept the period derived from the G_p spectrum as solar related. We therefore feel that the results of our preliminary analysis are significant at approximately 98%. We do not feel that the preliminary analysis establishes a connection between the vorticity area index and solar activity; however, we do feel the analysis provides additional evidence for such a connection.

We intend to check the results of our analysis by analyzing the vorticity data taking account of the eccentricity of the earth's orbit as discussed in Section 3 of this report. We also intend to explore the possibility of other theoretical methods of estimating the statistical significance of the results providing more realistic estimates.

Table 1.

Period	F_{min}
27.49	9.07
19.88	8.37
44.28	7.58
19.65	6.87
29.57	5.77

Table of the five largest peaks in a tabulation of the lesser of the two F statistics for both G_p and vorticity spectra.

Table 2

Period	Larger Probability
19.88	26/1921
27.49	27/1921
44.52	27/1921
29.57	53/1921
37.58	71/1921

Table of the five most significant peaks in a tabulation of the empirical probability estimates for both G_p and vorticity spectra.

References

Abramowitz, M. and Stegun, I.A. 1970, Handbook of Mathematical Functions, National Bureau of Standards Applied Mathematics Series 55, pp. 946-989.

Bartels, J. 1932, Terr. Mag. Atm. Elect. 37, 1.

Chree, C. and Stagg, J.M. 1927, Phil. Trans. Roy. Soc. London, A 227 , 21.

Maunder, E.W. 1904a, M.N.R.A.S. 65, 2.

_____, 1904b, M.N.R.A.S. 65, 538.

Ness, N.F. and Wilcox, J.M. 1967, Solar Phys. 2, 351.

Newton, H.W. and Nunn, M.L. 1951, M.N.R.A.S. 111, 413.

Schatten, K.E. and Wilcox, J.M. 1967, J.G.R. 72, 5185.

Wilcox, J.M. 1968, Space Sci. Rev. 8, 258.

Wilcox, J.M. and Coburn, D.S. 1972, J.G.R. 77, 751.

Wilcox, J.M., Scherrer, P.H., Svalgaard, L., Roberts, W.O. and Olson, R.H. 1973, Science 180, 185.

Wilcox, J.M., Svalgaard, L. and Scherrer, P.H. 1975, Nature 225, 539.

5. Stochastic Acceleration in Solar Flares
(C.E. Newman)

The preliminary studies of the viability of stochastic acceleration by MHD turbulence as a possible Phase 2 ion production mechanism in solar flares, as given in the last status report (Newman, 1975), have been modified to allow consideration of a particular model for the turbulent spectrum and supplemented by numerical calculations of the solutions. As mentioned in that report, a power-law frequency spectrum with index ν for the turbulence results in an equation for the ion energy distribution which admits a power-law with index $n = \frac{1}{2}(\nu - 1)$ as a steady-state solution. The attractiveness of stochastic acceleration as the ion production mechanism depends then upon how well it can provide answers to the following questions:

1. For reasonable plasma parameters, characteristic of solar flares, does the ion distribution approach the power-law steady-state solution on a time-scale consistent with the observed 5 - 20 min. lifetimes of such bursts?
2. Are the observed ion energies of 100 - 1000 MeV explained by this mechanism?
3. Can it explain the enhanced abundances of heavier ions in these bursts?

In order to obtain the answers to the above questions, we have assumed a specific model for the turbulence. In this model the frequency spectrum is a power-law with upper and lower cut-off frequencies ω_ℓ and ω_u respectively:

$$S(\omega) \propto \omega^{-\nu} \text{ for } \omega_\ell \leq \omega \leq \omega_u$$

$$S(\omega) = 0 \quad \text{for } \omega < \omega_\ell \text{ or } \omega > \omega_u$$

Since acceleration by MHD turbulence takes place via the quasi-linear wave-particle interaction at cyclotron resonance (Newman, 1972), it follows that only ions with energies in the range $E_o \leq E \leq (\omega_u/\omega_\ell)^2 E_o = E_f$ are accelerated by the turbulence. The injection energy E_o (in MeV) is given by

$$E_o = 2.5 \times 10^4 \; Z^2 \; A^{-1} \left(\frac{\Omega_H}{\omega_u}\right)^2 B^2 \; n_e^{-1} \quad ,$$

where Z and A are the charge and mass numbers of the ion, $\Omega_H = \frac{eB}{m_p c}$ is the proton gyrofrequency, B is the magnetic field strength in gauss, and n_e is the electron number density in cm^{-3}.

The energy-space quasi-linear diffusion equation for the ion distribution N(E,t) becomes (Newman, 1973), under these assumptions and the additional condition that $E_f >> E_o$,

$$\frac{1}{D}\frac{\partial}{\partial t} N(E,t) = -\left(n + \frac{3}{2}\right)\frac{\partial}{\partial E}\left(E^n N\right) + \frac{\partial^2}{\partial E^2}\left(E^{n+1} N\right), \quad E_o < E \qquad (1)$$

where $n = \frac{1}{2}(\nu - 1)$, the diffusion coefficient $D = \left(\frac{2}{n-1}\right)^2 E_o^{1-n} \; t_A^{-1}$, and the characteristic time t_A (in seconds) is given by

$$t_A = 2.2 \times 10^{-5} \; \frac{(2n+1)(2n+3)^2}{n(n-1)^2} \left(\frac{\Omega_H}{\omega_u}\right)^2 \frac{\epsilon_B}{\epsilon_T} \left(\frac{E_f}{E_o}\right)^n B^{-1} \; Z \; A^{-1} \qquad (2)$$

The quantity $\frac{\epsilon_T}{\epsilon_B}$ appearing in (2) is the ratio of the total energy density of turbulence to the magnetic field energy density $\frac{B^2}{8\pi}$.

The solution to (1) with boundary conditions

$$N(E, 0) = N_o\left(\frac{E}{E_o}\right)^{-\alpha} \quad , \quad N(E_o, t) = N_o, \quad N(\infty, t) = 0 \quad ,$$

was given in reference 1. This solution as a function of energy is plotted for various values of $\tau = t/t_A$ in Figure 1, where n and α are taken as 2.5 and 5.5 respectively. It is easily seen from this figure that the steady-state solution is nearly reached at time $\tau = 0.1$.

It is now possible to provide the answer to the questions enumerated above. As parameters typical of a reconnection region, we take

$$B = 30 \text{ gauss}, \quad \left(\frac{\Omega_H}{\omega_u}\right)^2 = 10^3, \quad \frac{\epsilon_T}{\epsilon_B} = 0.1, \quad n_e = 10^9 \text{ cm}^{-3}, \quad \frac{E_f}{E_o} = 40 \ .$$

We find that the injection energy E_o is thus given by

$$E_o = 25 \ Z^2 \ A^{-1} \text{ MeV} \ ,$$

and the highest energy attainable E_f by

$$E_f = 1000 \ Z^2 \ A^{-1} \text{ MeV}.$$

The characteristic time t_A becomes

$$t_A = 5 \times 10^3 \ Z \ A^{-1} \text{ sec.}$$

so that the time required for a steady state to be achieved is

$$t \sim 0.1 \ t_A = 500 \ Z \ A^{-1} \text{ sec.}$$

Thus the answers to questions (1) and (2) are definitely affirmative.

To answer question (3), we can show that for $t \gtrsim 0.1 \ t_A$ the total number density of particles N_A accelerated above by this mechanism is given by

$$\frac{N_A}{N} = 24\ t/t_A + 0.4 \quad ,$$

where

$$N = \int_{E_o}^{\infty} N_o(E,0)\ dE$$

is the total number density of particles above E_o at t = 0. Since t_A^{-1} varies as AZ^{-1}, we see that the heavier the ion, the greater the number (relative to the original density) accelerated above E_o. Hence the last question can also be answered in the affirmative.

For these reasons we conclude that MHD turbulence is an attractive mechanism for acceleration of energetic ions in Phase 2. However, it cannot explain acceleration of thermal ions (≈ few KeV) to the 100 - 1000 MeV range since the factor $(E_f/E_o)^n$ in equation (2) becomes too large and gives values for t_A which are much too long. Thus some kind of injection (or preacceleration) mechanism is required to produce ions with energies ~ 25 MeV in order for stochastic acceleration to become effective. Possible injection mechanisms will be evaluated and presented at a future date.

References

Newman, C.E. 1972, Stanford University Institute for Plasma Research Report No. 461.

_____. 1973, J. Math. Phys. 14, 502.

_____. 1975, NASA Semiannual Report No. 6.

Figure Caption

Figure 1: The quantity $N(E, t)/N_o$, where N is the solution to equation (1), is plotted versus E/E_o for various values of $\tau = t/t_A$.

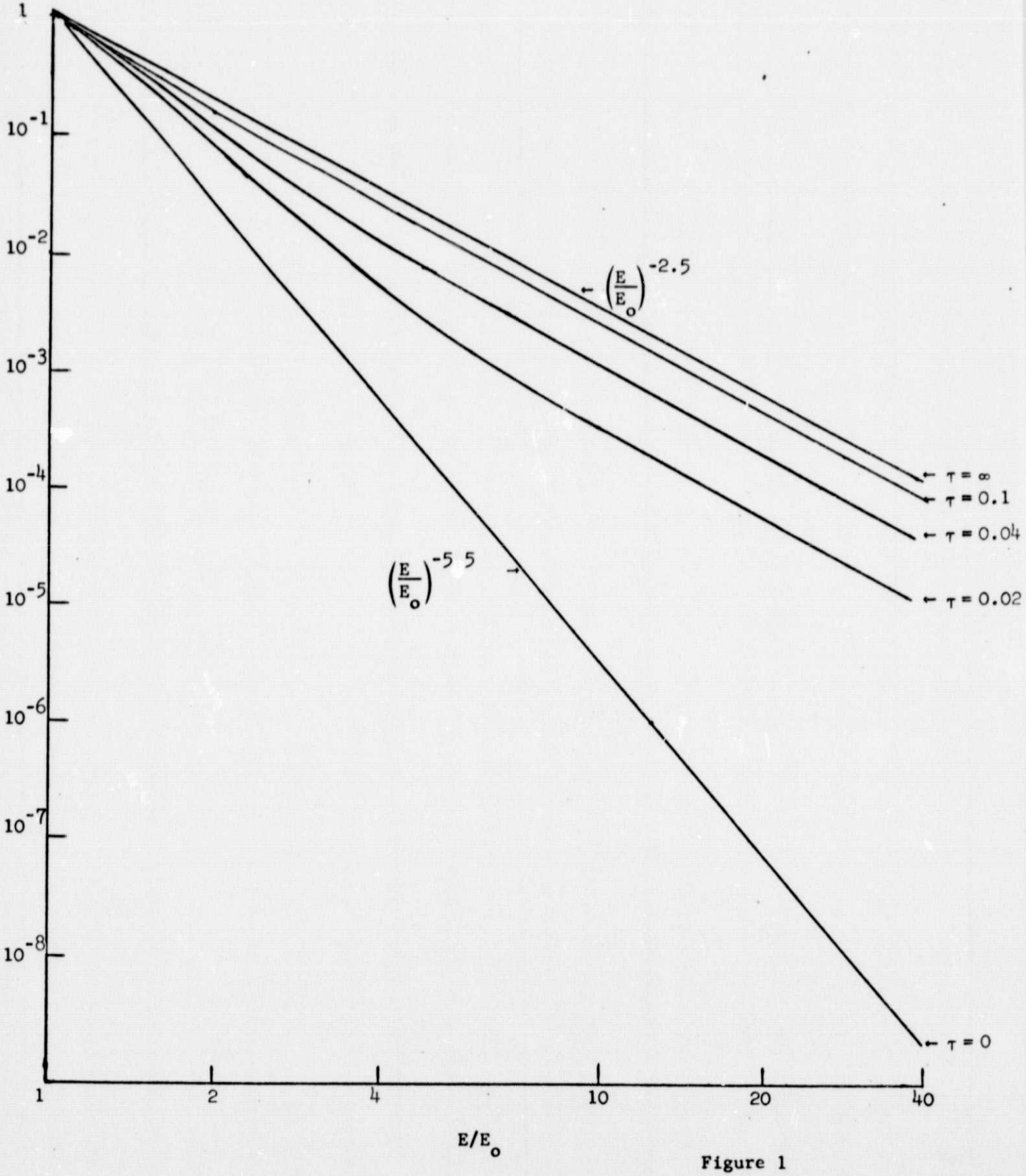
1
10^{-1}
10^{-2}
10^{-3}
10^{-4}
10^{-5}
10^{-6}
10^{-7}
10^{-8}
$\left(\frac{E}{E_o}\right)^{-2.5}$
$\left(\frac{E}{E_o}\right)^{-5.5}$
$\tau = \infty$
$\tau = 0.1$
$\tau = 0.04$
$\tau = 0.02$
$\tau = 0$
1
2
4
10
20
40
E/E_o

Figure 1

6. Analysis of Hard X-Rays from Solar Flares
(B.J. Lipa and V. Petrosian)

In large solar flares, particles are accelerated in at least two distinct phases. In the flash phase, electrons are repeatedly accelerated over short time intervals; in the second, they are accelerated to high energies, possibly by a shock wave which interacts with solar magnetic fields to create conditions under which Fermi acceleration occurs. Evidence for such a shock wave emerges from a study of pulsations which have been observed to modulate the radio continuum during solar flares (Achong, 1974). In the mechanism which has been proposed to explain these effects (Rosenberg, 1970), a Type II shock wave intercepts a magnetic flux tube that loops the corona. When the shock wave reaches the top of the arch, the tube is excited into radial oscillations and the resulting magnetic field oscillations produce pulsed modulation in synchrotron radiation. The same process can occur lower in the solar atmosphere, where modulation in the density produces pulsations in bremsstrahlung radiation.

We have begun a study of hard x-ray emission, using data from the OSO-5 satellite. To search for periodicities, maximum-entropy spectral analysis was used. Four flares have been analyzed and the results are summarized as follows.

March 1, 1969

The flash phase consists of strictly periodic bursts of period 39 seconds, which were observed to 111 KeV. Following the impulsive phase, thermal radiation dominates; no oscillations are observed.

March 21, 1969

The flash phase consists of quasi-periodic impulsive bursts, separated by approximately 400 seconds. Superimposed on this were oscillations which were indicated by highly significant double peaks in the frequency spectrum with periods of 24 and 33 seconds. No oscillations were observed in a second acceleration phase.

March 30, 1969

The flash phase is extremely rapid and there is some evidence for short-period (8 seconds) oscillations. In the succeeding second acceleration process, no oscillations occur.

November 5, 1970

Quasi-periodic bursts separated by approximately 140 seconds dominate the first half of the event. Superimposed upon these are oscillations indicated by a highly significant peak in the frequency spectrum. The period varied between 29 and 48 seconds as the impulsive phase proceeded.

It appears from this limited analysis that the first acceleration phase often consists of quasi-periodic bursts due perhaps to repetitive instabilities occurring in the magnetic field. Superimposed on these bursts are modulations which may be due to the modulation of the flux tube density described above.

There is a difficulty in interpreting the periods found due to the manner in which the x-ray data was collected. The measurements were collected from the rotating wheel of the spacecraft by sampling the solar burst for .19 seconds during every period of revolution of 1.91 seconds. It is therefore possible that the observed period is

a beat period with the revolution time. However, the periods obtained are of the same order of magnitude as the 16-second period observed by Parks and Winckler (1971).

We intend to make a statistical study of x-ray data from a large number of flares. We intend to find the electron spectrum responsible for the x-ray bursts, the relation between the energy emitted and the periods involved, and the polarization of the resulting x-rays. We will also look for associated behavior in other solar phenomena. In particular we will look for pulsations at microwave and meter wavelengths, and the relation between pulsating structures, Type II bursts and particle emission.

References

Achong, A. 1974, Solar Phys. 37, 477.

Parks, G.K. and Winckler, J.R. 1971, Solar Phys. 16, 186.

Rosenberg, H. 1970, Astron. Astrophys. 9, 159.

7. Solar X-Rays
(V. Petrosian)

As described in the previous semiannual report, the predictions of our model of the impulsive hard x-ray bursts are consistent with all observed properties of these bursts. This agreement is a consequence of the beaming of the x-ray-generating electrons toward the chromosphere. Because of the relativistic beaming of the bremsstrahlung radiation in the direction of electron motion, most of the radiation would be directed toward the chromosphere. This beaming becomes more important at higher energies. The reflection of the photons directed toward the sun could in certain cases contribute significantly to the observed radiation.

We have devised a Monte Carlo procedure for calculation of the x-ray albedo of the solar atmosphere, for different x-ray energies and different incident angles. The accuracy of this procedure has been determined by comparing results from it with analytic solutions for a few cases where such solutions are possible. The results of this calculation would enable us to determine the center-to-limb variation with solar longitude of the energy spectral index, the frequency of occurrence, and the ratio of hard-to-soft x-ray intensities as described previously (Petrosian, 1975). These results are being prepared for publication.

We intend to extend this program for calculation of polarization properties of the reflected radiation. There have been calculations of the polarization of x-rays from an electron beam (Haug, 1972 and Brown, 1973), but unfortunately only calculation of polarization of the photons emitted directly toward the earth has been published.

However, in order to determine the polarization state of the total (direct and reflected) x-rays we need to calculate first the polarization state of the x-rays emitted toward the sun. These calculations are under way. The results of this calculation will be used in the Monte Carlo program for determination of the polarization state of the reflected photons.

References

Brown, J.C. 1972, Solar Phys. 26, 441.

Haug, E. 1972, Solar Phys. 25, 425.

Petrosian, V. 1975, Ap. J. 197, 235.